

Magnetic order of the hexagonal rare-earth manganite $\text{Dy}_{0.5}\text{Y}_{0.5}\text{MnO}_3$

Joel S. Helton,^{1,*} Deepak K. Singh,^{1,2} Harikrishnan S. Nair,³ and Suja Elizabeth⁴

¹*NIST Center for Neutron Research, National Institute of Standards and Technology, Gaithersburg, Maryland 20899, USA*

²*Department of Materials Science and Engineering, University of Maryland, College Park, Maryland 20742, USA*

³*Jülich Centre for Neutron Science, Forschungszentrum Jülich, Outstation at FRM-II, D-85747 Garching, Germany*

⁴*Department of Physics, Indian Institute of Science, Bangalore 560012, India*

(Received 3 June 2011; published 26 August 2011)

Hexagonal $\text{Dy}_{0.5}\text{Y}_{0.5}\text{MnO}_3$, a multiferroic rare-earth manganite with geometrically frustrated antiferromagnetism, has been investigated with single-crystal neutron diffraction measurements. Below 3.4 K magnetic order is observed on both the Mn (antiferromagnetic) and Dy (ferrimagnetic) sublattices that is identical to that of undiluted hexagonal DyMnO_3 at low temperature. The Mn moments undergo a spin reorientation transition between 3.4 K and 10 K, with antiferromagnetic order of the Mn sublattice persisting up to 70 K; the antiferromagnetic order in this phase is distinct from that observed in undiluted (h) DyMnO_3 , yielding a qualitatively new phase diagram not seen in other hexagonal rare-earth manganites. A magnetic field applied parallel to the crystallographic c axis will drive a transition from the antiferromagnetic phase into the low-temperature ferrimagnetic phase with little hysteresis.

DOI: [10.1103/PhysRevB.84.064434](https://doi.org/10.1103/PhysRevB.84.064434)

PACS number(s): 75.25.-j, 75.85.+t, 75.50.Ee, 75.47.Lx

I. INTRODUCTION

The crystalline structure of rare-earth manganites (RMnO_3 with $R = \text{Y}$, Sc, or a lanthanide) is determined by the ionic radius of the R^{3+} cation. Materials with a large R^{3+} ionic radius ($R = \text{La}$ through Tb) crystallize in an orthorhombic perovskite structure, while materials with a smaller R^{3+} ionic radius ($R = \text{Y}$, Sc, or Ho through Lu)^{1–6} crystallize in a hexagonal structure. DyMnO_3 typically crystallizes in the orthorhombic structure,⁷ but with proper growth conditions hexagonal (h) DyMnO_3 can be stabilized.^{8,9} The hexagonal rare-earth manganites, (h) RMnO_3 , are paraelectric at very high temperatures but display a structural transition ($T_C \approx 1000$ K) to a ferroelectric phase with the noncentrosymmetric $P6_3cm$ space group.¹⁰ The (h) RMnO_3 materials feature slightly distorted triangular lattice planes of Mn ions; the antiferromagnetic nearest-neighbor exchange interaction leads to geometrically frustrated magnetism. Below a Néel temperature of ≈ 100 K these materials are magnetically ordered, with easy-plane antiferromagnetic order of the Mn sublattice coexisting with the ferroelectric order. Many hexagonal rare-earth manganites display one or more spin reorientation transitions of the Mn moments at lower temperatures^{11,12} or under an applied field;^{13,14} the R ions also form distorted triangular lattice planes and, for magnetic ions, will order along the c axis. Several of these materials have attracted interest because of significant magnetoelectric^{15,16} or magnetoelastic¹⁷ effects. Despite the structural similarities between the various members of the (h) RMnO_3 family, the magnetically ordered structures often differ, with structures that transform according to each of the four one-dimensional irreducible representations of the point group observed in at least one material. The dependence of the magnetic ordering of the Mn sublattice on the rare-earth element has been attributed to the ionic radius of the R^{3+} cation¹⁸ or a biquadratic $3d-4f$ magnetic coupling.¹⁹

Hexagonal (h) DyMnO_3 , with the largest rare-earth ionic radius of this series, features an interesting magnetic phase diagram.^{9,19,20} In the low-temperature phase (below ≈ 8 K)

both the Mn and Dy sublattices are magnetically ordered according to the Γ_2 irreducible representation. At a temperature of 8 K the Mn moments undergo a spin reorientation transition and are ordered in the Γ_4 representation up to 68 K.¹⁹ X-ray resonant magnetic scattering measurements also find a weak Dy moment in this temperature range, ordered according to the Γ_3 representation.²⁰ This incompatible order, with different irreducible representations present on the two sublattices, calls into question long-standing assumptions about the rigidity of the $3d-4f$ interaction in (h) RMnO_3 materials.¹⁹ YMnO_3 features magnetism only on the Mn sublattice and is known to order in the Γ_3 irreducible representation below $T_N \approx 75$ K.²¹ YMnO_3 has also been reported to feature large magnetoelastic effects¹⁷ and coupling between electric and magnetic domains.²² Compounds where magnetic rare-earth ions are partially replaced with nonmagnetic Y^{3+} ions, such as $\text{Ho}_{1-x}\text{Y}_x\text{MnO}_3$ ^{23,24} and $\text{Er}_{1-x}\text{Y}_x\text{MnO}_3$,^{25,26} allow for further examination of the role that the rare-earth ions play in determining the magnetic structure and open up the possibility of novel phase diagrams not observed in undoped compounds. We report single-crystal neutron diffraction studies of hexagonal $\text{Dy}_{0.5}\text{Y}_{0.5}\text{MnO}_3$ (DYMO) and find evidence for a spin reorientation transition not seen in other hexagonal rare-earth manganites at zero field.

II. EXPERIMENT

Large, high-quality single-crystal samples of $\text{Dy}_{0.5}\text{Y}_{0.5}\text{MnO}_3$ were prepared as previously reported.²⁷ DYMO crystallizes in the hexagonal $P6_3cm$ space group (#185) with lattice parameters (at 300 K) of $a = b = 6.161(1)$ Å and $c = 11.446(2)$ Å. As in other hexagonal rare-earth manganites, Mn^{3+} ions ($S = 2$) occupy the $6c$ positions at $(x, 0, 0)$ with $x \approx \frac{1}{3}$. A material with $x = \frac{1}{3}$ would feature perfect triangular lattice planes; in DYMO $x = 0.3379(4)$ yielding a slightly distorted triangular lattice. The rare-earth R^{3+} ions occupy two crystallographically distinct sites, at the $2a$ and $4b$ Wyckoff positions and also form distorted triangular lattice planes. In DYMO the rare-earth

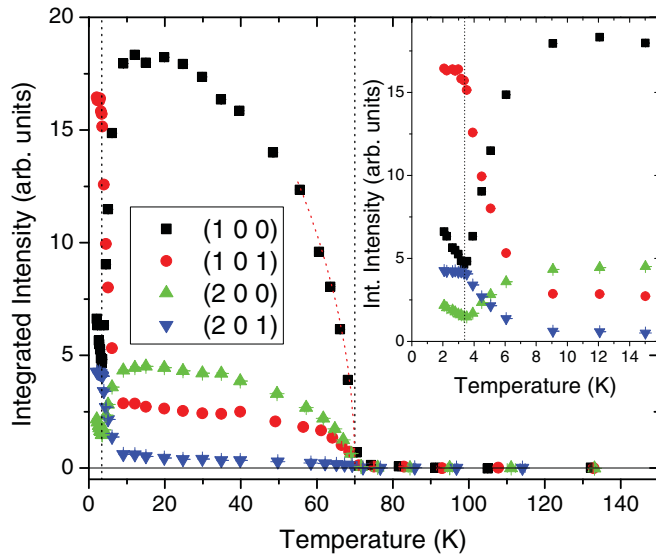


FIG. 1. (Color online) Integrated magnetic intensities of the (1 0 0), (1 0 1), (2 0 0), and (2 0 1) Bragg reflections as a function of temperature. All data were measured while warming. The inset shows a closer view of the low temperature portion of the graph. Transitions are observed at $T_N^{\text{Mn}} = 70$ K and $T_N^{\text{Dy}} = 3.4$ K; these temperatures are designated with dashed vertical lines. The red dotted line reflects a fit of the (1 0 0) intensity to an order parameter form with $\beta = 0.25 \pm 0.05$. Error bars throughout this article are statistical in nature and represent one standard deviation.

sites are occupied with equal probability by nonmagnetic Y^{3+} ions and ${}^6\text{H}_{15/2} \text{Dy}^{3+}$ ions ($gJ = 10 \mu_B$), as determined by x-ray powder diffraction on crushed single crystals.²⁷ Previously reported specific heat measurements found peaks at 3 K and 68 K; analogously with other hexagonal rare-earth manganites such as DyMnO_3 , it was suggested that these peaks correspond to the onset of antiferromagnetic order of the Mn lattice, $T_N^{\text{Mn}} \approx 68$ K, and ferrimagnetic order of Dy moments on the rare-earth lattice, $T_N^{\text{Dy}} \approx 3$ K.

Neutron diffraction experiments were carried out using the BT9 thermal triple-axis spectrometer at the NIST Center for Neutron Research. The neutron initial and final energies were selected using the (0 0 2) reflection of the pyrolytic graphite (PG) monochromator and analyzer. We used 40'-47'-40' open collimation as well as PG filters to reduce contamination of the beam with higher-order neutron wavelengths. The detailed temperature dependence of four magnetic reflections (shown in Fig. 1) was measured using a large (≈ 1 g) single crystal mounted in the (H 0 L) scattering plane at a fixed neutron energy of 30.5 meV ($\lambda = 1.64$ Å). Refinement of the ordered moments utilized diffraction measurements taken at temperatures of 1.6 K, 25 K, and 120 K at a fixed neutron energy of 30.5 meV. In order to minimize absorption of neutrons by the sample, these measurements were taken with small single crystals: an 8-mg sample mounted in the (H 0 L) scattering plane and a 6-mg sample mounted in the (H K 0) scattering plane. Some magnetic reflections also featured weak nuclear contributions which were removed by subtracting the 120 K intensity; the Debye-Waller factor has been ignored, which is justifiable, given that the intensities of nuclear Bragg peaks with no magnetic intensity [such as (0 0 L) where L

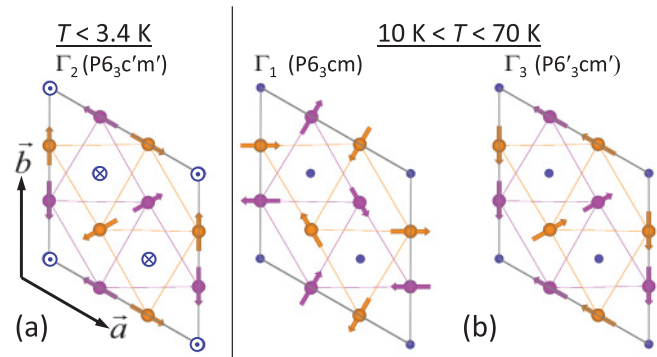


FIG. 2. (Color online) (a) Magnetic structure in the low-temperature ferrimagnetic phase, present below $T_N^{\text{Dy}} = 3.4$ K. The structure belongs to the $P6_3c'm'$ magnetic space group (Γ_2 irreducible representation). Mn ions at $z = 0$ are shown in purple, Mn ions at $z = 1/2$ are shown in orange, and the rare-earth ions are shown in blue. The refined ordered moments are $3.7 \pm 0.4 \mu_B$ on the Mn ions and $3.1 \pm 0.3 \mu_B$ on the Dy ions. (b) The two possible magnetic structures for the antiferromagnetic phase: $P6_3cm$ magnetic space group (Γ_1 irreducible representation) on the left and $P6_3c'm'$ magnetic space group (Γ_3) on the right. The Mn ordered moment is $3.5 \pm 0.4 \mu_B$. Any Dy ordered moment in this temperature range is too small to be measured by neutron diffraction. The structural unit cell is outlined in gray.

is even] remained constant within the statistical uncertainties between 1.6 K and 120 K. The scattering intensity in absolute units, and from this the value of the ordered moments, was determined by normalizing the intensities of nuclear Bragg peaks measured at 120 K to the calculated nuclear intensities. The intensities of the (1 0 0) and (3 $\bar{1}$ 0) reflections in a magnetic field were measured on the 6-mg sample mounted in the (H K 0) scattering plane; the sample was placed inside a helium flow dewar with a minimum temperature of 4 K inserted into a 7-T vertical field superconducting magnet. These data were taken at a fixed neutron energy of 14.7 meV ($\lambda = 2.36$ Å). All neutron diffraction data are reported in terms of the integrated intensity, integrated over a rocking curve (θ scan) through the peak position.

The allowed magnetic structures in DYMO correspond to the six irreducible representations of the $P6_3cm$ space group with propagation vector $\vec{k} = 0$; as in other hexagonal rare-earth manganites, only the four one-dimensional irreducible representations (designated as Γ_1 through Γ_4) are required to describe the observed structures.^{28,29} For each of these representations the Mn sublattice displays antiferromagnetic order within the ab plane, with the three spins around any triangle oriented 120° apart. The R^{3+} sublattice is ordered along the crystallographic c axis. The rare-earth $4b$ sites are antiferromagnetically ordered for the Γ_1 , Γ_3 , and Γ_4 representations; the $2a$ rare-earth sites are antiferromagnetically ordered in the Γ_3 representation and paramagnetic for the Γ_1 and Γ_4 representations. The $2a$ and $4b$ sites are each ferromagnetically ordered in the Γ_2 representation, with the coupling between the two sites yielding either ferromagnetism or ferrimagnetism. In phases where only the Mn sublattice is magnetically ordered a hexagonal rare-earth manganite with $x = \frac{1}{3}$ (featuring undistorted triangular lattice planes) would have perfectly identical neutron-scattering structure factors

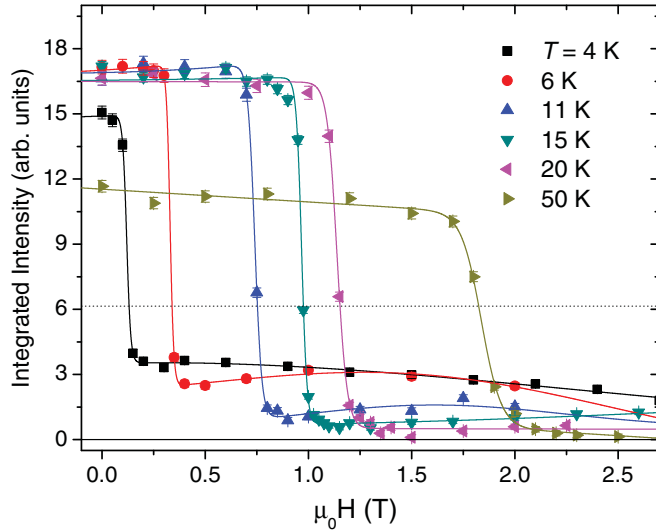


FIG. 3. (Color online) Integrated intensity of the (1 0 0) peak as a function of field. The data were taken while increasing field. Lines are a guide to the eye. The dotted horizontal line represents the expected intensity at 2 K in zero field.

in either the Γ_1 or Γ_3 representations, as well as in the Γ_2 or Γ_4 representations. Unambiguous differentiation between these homometric magnetic structures requires complementary measurement techniques such as optical second harmonic spectroscopy.^{1,21,30} The distortion of the triangular planes leads to some variation in the neutron-scattering structure factors; however, these results, from single-crystal diffraction measurements on a strongly absorbing sample, will not be able to distinguish between the Γ_1 and Γ_3 structures.

III. RESULTS

A. Zero-field magnetic order

Figure 1 displays the temperature dependence of the integrated intensities of the (1 0 0), (1 0 1), (2 0 0), and (2 0 1) Bragg reflections measured while warming from 2.1 K to 130 K. The background and any high temperature nuclear contributions to the intensities have been subtracted. At 2.1 K all four reflections display magnetic intensity, with the (1 0 1) reflection the strongest. Between 2.1 K and 3.4 K the measured intensities of the (H 0 1) reflections remain relatively constant while those of the (H 0 0) reflections steadily decrease with increasing temperature, with an intensity at 3.4 K that is about 68% of the base temperature intensity. On increasing the temperature beyond 3.4 K, the intensities of the (H 0 0) peaks steadily increase while the intensities of the (H 0 1) peaks decrease so that the (1 0 0) reflection becomes the strongest measured; this rapid change in intensity persists only to around 10 K. This will be shown to correspond to a spin reorientation transition of the Mn moments and perhaps explains the 10 K anomaly reported²⁷ in the derivative of $1/\chi$. Above 10 K the intensities of all peaks slowly decrease until reaching zero at 70 K. The intensity can be fit to an order parameter form: $I(T) \propto (|T - T_N|/T_N)^{2\beta}$. The dotted red line in Fig. 1 is a fit of the (1 0 0) intensity to this form with $\beta = 0.25 \pm 0.05$.

Table I displays the calculated magnetic intensities for the reflections shown in Fig. 1 with the largest reflection

TABLE I. Calculated magnetic scattering intensities for the reflections displayed in Fig. 1. The most intense reflection in each column has been normalized to 100. In the low-temperature phase below 3.4 K the data are consistent with Γ_2 order for both the Mn and Dy sublattice. In the antiferromagnetic phase between 10 K and 70 K the data are consistent with Mn sublattice order in either the Γ_1 or Γ_3 irreducible representation.

	Mn order				Dy order
	Γ_1	Γ_2	Γ_3	Γ_4	Γ_2
(1 0 0)	100	0	100	0	100
(1 0 1)	17	100	15	100	0
(2 0 0)	32	0	27	0	38
(2 0 1)	1	26	1	33	0

in each column normalized to 100. The reported intensities reflect the calculated magnetic cross section corrected for the resolution function of a triple-axis neutron spectrometer. Calculated intensities are shown for Mn moments ordered in each of the four one-dimensional irreducible representations, as well as for Dy moments ordered in the Γ_2 representation. Previous magnetization measurements on DYMO²⁷ with $\vec{H} \parallel \vec{c}$ revealed a low-temperature state with a spontaneous magnetization of $\approx 0.5 \mu_B$ per formula unit (measured at 2 K). Of the four irreducible representations present in hexagonal rare-earth manganites only the Γ_2 structure is consistent with either ferrimagnetism or ferromagnetism; undoped hexagonal DyMnO₃ is ferrimagnetic at low temperatures and is known to order in the Γ_2 representation.²⁰ When ordering in the Γ_2 structure the magnetic cross sections of the (H 0 1) reflections depend only on the ordered moment of the Mn ions while those of the (H 0 0) reflections depend only on the ordered moment of the Dy ions. The Mn ordered moment is therefore found to be almost temperature independent below 3.4 K, while the Dy ordered moment decreases continuously with increasing temperature between 2.1 K and 3.4 K.

Assuming a ferrimagnetic structure with ordered moments on the $2a$ and $4b$ sites that are antiparallel but equal in magnitude, a refinement of magnetic reflections measured at 1.6 K reveals ordered moments of $3.7 \pm 0.4 \mu_B$ for the Mn ions and $3.1 \pm 0.3 \mu_B$ for the Dy ions ($1.6 \pm 0.2 \mu_B$ for each rare-earth site). This structure is displayed in Fig. 2(a) (The crystal structures shown in Fig. 2 were produced using VESTA.³¹) When magnetic domains are fully aligned this ordered moment will lead to a net magnetization of $3.1 \pm 0.3 \mu_B$ per unit cell (or $0.52 \pm 0.05 \mu_B$ per formula unit) along the crystallographic c axis, which is consistent with the reported bulk spontaneous magnetization.²⁷ Allowing for different ordered moments on the Dy $4b$ and $2a$ sites did not appreciably improve the fit of the 1.6 K data, nor could allowing for different moments on these sites produce a comparably good fit while yielding a net moment consistent with magnetization measurements. A ferromagnetic ground state can likewise be excluded. A ferromagnetic state with equal ordered moments on the $2a$ and $4b$ sites would give no intensity for the (H 0 0) reflections; when ordering in the Γ_2 structure the intensities of these reflections depend on the difference in moment at the rare-earth sites: $I(\vec{Q}_{H00}) \propto |\vec{M}_{4b} - \vec{M}_{2a}|^2$, where the ordered moments on the $2a$ and $4b$ sites are \vec{M}_{2a} and \vec{M}_{4b} . A ferromagnetic

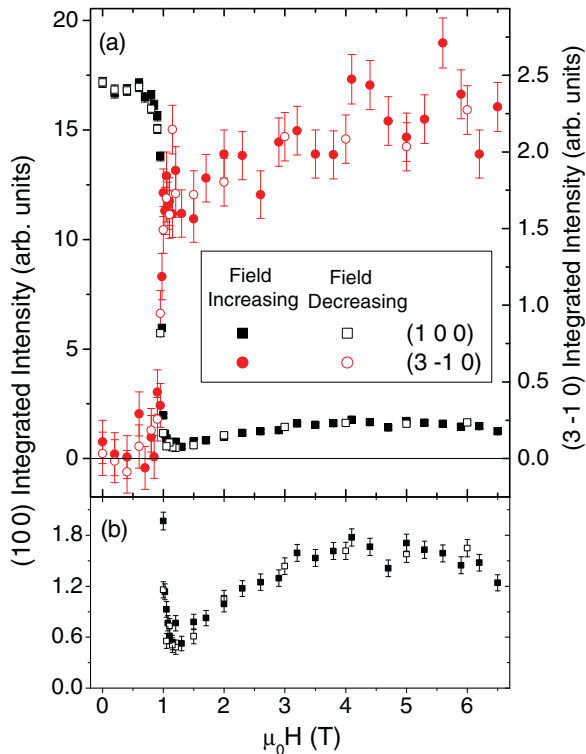


FIG. 4. (Color online) (a) Integrated intensities of the (1 0 0) (left scale) and (3 $\bar{1}$ 0) (right scale) peaks measured at $T = 15$ K. Solid symbols represent measurements taken with increasing field, and open symbols represent those taken with a decreasing field. (b) Detail of the high-field region for the (1 0 0) intensity.

state with different ordered moments on the $2a$ and $4b$ sites is consistent with the neutron diffraction data only while yielding a net moment inconsistent with magnetization measurements. The Mn ordered moment at 1.6 K is close to the full moment value; however, the Dy ordered moment is considerably reduced from the full $10 \mu_B$ value of the ${}^6H_{15/2}$ Dy^{3+} ions. The low temperature magnetization in undoped DyMnO_3 would suggest a similarly reduced ordered moment for the Dy ions in the ferrimagnetic phase.⁸

The magnetic structure in the antiferromagnetic phase ($10 \text{ K} < T < 70 \text{ K}$) is consistent with an ordered moment on only the Mn sublattice, with order according to either the Γ_1 or Γ_3 irreducible representation. These magnetic structures are shown in Fig. 2(b). It should be noted that neither of these possibilities are consistent with the structure of the Mn moments in (h) DyMnO_3 , which order in the Γ_4 representation above the low-temperature ferrimagnetic phase.¹⁹ A refinement of magnetic reflections measured at 25 K gives an ordered moment of $3.5 \pm 0.4 \mu_B$ for the Mn sublattice. The ordered moment at 25 K is comparable in size to that determined at 1.6 K, suggesting a spin reorientation transition where Mn spins rotate between 3.4 K and 10 K with little change in magnitude. Element specific x-ray resonant magnetic scattering measurements on hexagonal DyMnO_3 ²⁰ and HoMnO_3 ³² have reported a weak rare-earth moment at comparable temperatures, induced by a splitting of the ground-state crystal field doublet. While DYMO might similarly feature a weak Dy ordered moment in this temperature range,

neutron-scattering measurements will be sensitive to only the much larger ordered moment of the Mn sublattice and the refinement is not improved by allowing for an ordered moment on the Dy sublattice at 25 K.

The magnetic structure of YMnO_3 is known to be the Γ_3 representation.²¹ If the antiferromagnetic phase of DYMO were likewise Γ_3 , the spin reorientation transition into the low-temperature Γ_2 phase would differ from the spin reorientation transitions previously observed in hexagonal rare-earth manganites. A magnetic structure in the Γ_1 irreducible representation can be transformed into the Γ_2 representation through a 90° counterclockwise rotation of all Mn moments. However, a transformation of a structure in the Γ_3 representation as shown in Fig. 2 into the Γ_2 representation would require a 180° rotation of only the Mn moments in the $z = \frac{1}{2}$ plane. In other hexagonal rare-earth manganites, it has been suggested³⁰ that spin reorientation transitions between the four irreducible representations occur via in-phase or antiphase rotations where the moments in adjacent Mn layers rotate with an equal (in-phase) or opposite (antiphase) direction. For example, the Mn moments in HoMnO_3 display an in-phase reorientation transition (Γ_4 to Γ_3) at $T \approx 40 \text{ K}$ and an antiphase transition (Γ_3 to Γ_1) at $T \approx 8 \text{ K}$, while the Mn moments in (h) DyMnO_3 display an antiphase rotation (Γ_4 to Γ_2) at $T \approx 8 \text{ K}$. Further, while materials such as ScMnO_3 ,² $\text{Er}_x\text{Y}_{1-x}\text{MnO}_3$,²⁵ and YMnO_3 under pressure¹⁸ have been reported to feature broad temperature ranges where the magnetic structure is not one of the four irreducible representations, the observed structures can still be described as an in-phase or antiphase rotation of all Mn moments away from one of the principal structures.

B. Field dependence of the magnetic order

Below $T_N^{\text{Dy}} = 3.4 \text{ K}$ DYMO is ferrimagnetic with a spontaneous net magnetization. Above T_N^{Dy} , $M(H)$ curves display symmetric magnetization steps at a critical field value that increases with temperature; the size of these steps decreases with increasing temperature, becoming immeasurably small around 40 K.²⁷ This behavior is remarkably similar to that previously reported in (h) DyMnO_3 ,⁸ but the moment increase associated with the magnetization steps in DYMO is about one half of the increase in (h) DyMnO_3 . Figure 3 displays the intensity of the (1 0 0) magnetic Bragg reflection as a function of field with $\vec{H} \parallel \vec{c}$ at temperatures between 4 K and 50 K, measured while increasing the field after zero field cooling. For each of these temperatures, we find a sudden drop in the (1 0 0) intensity at a critical field value that increases with temperature. As was shown in Fig. 1, the intensity of the (1 0 0) reflection will be much higher in the antiferromagnetic phase than in the low-temperature phase, such that this behavior is easily associated with a field-induced transition into the ferrimagnetic phase. The data definitively show a spin reorientation of the Mn moments along with the field-induced ferrimagnetic ordering of the Dy moments, as the intensity of this reflection would not drop if the Mn moments remained ordered in the original structure. The intensity of this reflection in the field-induced phase is weaker than in zero field at low temperature [the dotted horizontal line represents the expected intensity of the (1 0 0) reflection at 2 K and zero field]. This

likely arises from a considerably smaller Dy ordered moment, consistent with the smaller magnitude of the magnetization steps at higher temperatures in the $M(H)$ curves. Interestingly, neutron diffraction is sensitive enough that this transition is still clearly measurable in the 50 K data, while it could not be measured above 40 K in the magnetization data.²⁷

The field dependence of the intensities at the (1 0 0) and (3 $\bar{1}$ 0) reflections at $T = 15$ K is displayed in Fig. 4. In Fig. 4(a), both reflections show the expected transition at $\mu_0 H_c \approx 1$ T; data taken in rising and falling field show only a slight hysteresis, consistent with the small hysteresis of the magnetization steps in the bulk magnetization data. In addition to DYMO, undoped (h)DyMnO₃ displays little hysteresis while magnetization steps in ErMnO₃³³ display considerable hysteresis. The (3 $\bar{1}$ 0) reflection displays scattering in the low-temperature Γ_2 phase and very little scattering in the antiferromagnetic phase, such that this change in intensity is likewise consistent with a field-induced transition between the two. A more detailed view of the (1 0 0) intensity in the high-field region is shown in Fig. 4(b). Interestingly, the intensity of this peak rises slowly with increasing field up to about 4 T but then decreases with increasing field beyond 5 T. This likely reflects the evolution of the system from ferrimagnetic to ferromagnetic as the field is increased, as the fully polarized state (ferromagnetic with an equal moment for the 4a and 2b sites) would display no scattering at (1 0 0).

IV. SUMMARY

Below $T_N^{\text{Dy}} = 3.4$ K Dy_{0.5}Y_{0.5}MnO₃ is magnetically ordered in the Γ_2 irreducible representation with antiferromagnetic Mn order and ferrimagnetic Dy order. Between 3.4 K and 10 K we observe a spin reorientation transition of the Mn moments. Antiferromagnetic order of the Mn sites

persists up to $T_N^{\text{Mn}} = 70$ K. The magnetic structure of this phase is either Γ_1 or Γ_3 , inconsistent with the Γ_4 order observed in undiluted (h)DyMnO₃.¹⁹ In the antiferromagnetic phase, a magnetic field applied parallel to the c axis will drive a field-induced transition into the low-temperature ferrimagnetic phase with little hysteresis. Further knowledge of the different magnetic structures and reorientation transitions displayed by the Mn moments in various (h)RMnO₃ materials should lead to improved understanding of the unusual $3d$ - $4f$ magnetic coupling present in these materials.¹⁹ While the magnetic structure of the antiferromagnetic phase cannot be definitively determined from this experiment, it is clear that Dy_{0.5}Y_{0.5}MnO₃ displays a zero-field spin reorientation transition not previously observed in any other hexagonal rare-earth manganite. If the magnetic structure is Γ_3 , then the Γ_3 to Γ_2 spin reorientation transition would involve only half of the Mn ions in a manner not observed in other (h)RMnO₃ materials. The H - T phase diagram of HoMnO₃ features a boundary between Γ_1 and Γ_2 phases^{13,29} at $\mu_0 H \approx 2$ T, yet a zero field Γ_1 to Γ_2 spin reorientation transition has not been reported. Further work will be necessary to distinguish between the Γ_1 and Γ_3 structures in the antiferromagnetic phase and to determine if the domain walls arising from this unique spin reorientation will display magnetoelectric coupling as is observed in compounds such as HoMnO₃^{16,34} or YMnO₃.²²

ACKNOWLEDGMENTS

We thank J. W. Lynn for guidance and helpful discussions. J.S.H. acknowledges support from the NRC/NIST Postdoctoral Associateship Program. This work was supported in part by the National Science Foundation under Agreement No. DMR-0944772.

*joel.helton@nist.gov

¹D. Fröhlich, St. Leute, V. V. Pavlov, R. V. Pisarev, and K. Kohn, *J. Appl. Phys.* **85**, 4762 (1999).

²A. Muñoz, J. A. Alonso, M. J. Martínez-Lope, M. T. Casáis, J. L. Martínez, and M. T. Fernández-Díaz, *Phys. Rev. B* **62**, 9498 (2000).

³D. G. Tomuta, S. Ramakrishnan, G. J. Nieuwenhuys, and J. A. Mydosh, *J. Phys. Condens. Matter* **13**, 4543 (2001).

⁴H. Sugie, N. Iwata, and K. Kohn, *J. Phys. Soc. Jpn.* **71**, 1558 (2002).

⁵A. Muñoz, J. A. Alonso, M. J. Martínez-Lope, M. T. Casáis, J. L. Martínez, and M. T. Fernández-Díaz, *Chem. Mater.* **13**, 1497 (2001).

⁶F. Yen, C. R. dela Cruz, B. Lorenz, Y. Y. Sun, Y. Q. Wang, M. M. Gospodinov, and C. W. Chu, *Phys. Rev. B* **71**, 180407(R) (2005).

⁷O. Prokhnenko, R. Feyerherm, E. Dudzik, S. Landsgesell, N. Aliouane, L. C. Chapon, and D. N. Argyriou, *Phys. Rev. Lett.* **98**, 057206 (2007).

⁸V. Yu. Ivanov, A. A. Mukhin, A. S. Prokhorov, A. M. Balbashov, and L. D. Iskhakova, *Phys. Solid State* **48**, 1726 (2006).

⁹S. Harikrishnan, S. Rößler, C. M. Naveen Kumar, H. L. Bhat, U. K. Rößler, S. Wirth, F. Steglich, and Suja Elizabeth, *J. Phys. Condens. Matter* **21**, 096002 (2009).

¹⁰B. B. Van Aken, T. T. M. Palstra, A. Filippetti, and N. A. Spaldin, *Nat. Mater.* **3**, 164 (2004).

¹¹O. P. Vajk, M. Kenzelmann, J. W. Lynn, S. B. Kim, and S.-W. Cheong, *Phys. Rev. Lett.* **94**, 087601 (2005).

¹²Th. Lonkai, D. Wohlwein, J. Ihringer, and W. Prandl, *Appl. Phys. A* **74**, S843 (2002).

¹³B. Lorenz, F. Yen, M. M. Gospodinov, and C. W. Chu, *Phys. Rev. B* **71**, 014438 (2005).

¹⁴O. P. Vajk, M. Kenzelmann, J. W. Lynn, S. B. Kim, and S.-W. Cheong, *J. Appl. Phys.* **99**, 08E301 (2006).

¹⁵T. Lottermoser, T. Lonkai, U. Amann, D. Hohlwein, J. Ihringer, and M. Fiebig, *Nature* **430**, 541 (2004).

¹⁶B. G. Ueland, J. W. Lynn, M. Laver, Y. J. Choi, and S.-W. Cheong, *Phys. Rev. Lett.* **104**, 147204 (2010).

¹⁷S. Lee, A. Pirogov, M. Kang, K.-H. Jang, M. Yonemura, T. Kamiyama, S.-W. Cheong, F. Gozzo, N. Shin, H. Kimura *et al.* *Nature* **451**, 805 (2008).

¹⁸D. P. Kozlenko, S. Kichanov, S. Lee, J.-G. Park, and B. N. Savenko, *J. Phys. Condens. Matter* **19**, 156228 (2007).

¹⁹C. Wehrenfennig, D. Meier, Th. Lottermoser, Th. Lonkai, J.-U. Hoffmann, N. Aliouane, D. N. Argyriou, and M. Fiebig, *Phys. Rev. B* **82**, 100414(R) (2010).

- ²⁰S. Nandi, A. Kreyssig, J. Q. Yan, M. D. Vannette, J. C. Lang, L. Tan, J. W. Kim, R. Prozorov, T. A. Lograsso, R. J. McQueeney *et al.* *Phys. Rev. B* **78**, 075118 (2008).
- ²¹M. Fiebig, D. Fröhlich, K. Kohn, St. Leute, Th. Lottermoser, V. V. Pavlov, and R. V. Pisarev, *Phys. Rev. Lett.* **84**, 5620 (2000).
- ²²M. Fiebig, Th. Lottermoser, D. Fröhlich, A. V. Goltsev, and R. V. Pisarev, *Nature* **419**, 818 (2002).
- ²³H. D. Zhou, J. Lu, R. Vasic, B. W. Vogt, J. A. Janik, J. S. Brooks, and C. R. Wiebe, *Phys. Rev. B* **75**, 132406 (2007).
- ²⁴R. Vasic, H. D. Zhou, E. Jobilong, C. R. Wiebe, and J. S. Brooks, *Phys. Rev. B* **75**, 014436 (2007).
- ²⁵M. C. Sekhar, S. Lee, G. Choi, C. Lee, and J.-G. Park, *Phys. Rev. B* **72**, 014402 (2005).
- ²⁶O. P. Vajk, J. Gunasekera, Y. Wang, and T. Heitmann, *J. Appl. Phys.* **109**, 07D910 (2011).
- ²⁷Harikrishnan S. Nair, C. M. N. Kumar, H. L. Bhat, Suja Elizabeth, and Th. Brückel, *Phys. Rev. B* **83**, 104424 (2011).
- ²⁸W. Sikora and V. N. Syromyatnikov, *J. Magn. Magn. Mater.* **60**, 199 (1986).
- ²⁹I. Munawar and S. H. Curnoe, *J. Phys. Condens. Matter* **18**, 9575 (2006).
- ³⁰M. Fiebig, Th. Lottermoser, and R. V. Pisarev, *J. Appl. Phys.* **93**, 8194 (2003).
- ³¹K. Momma and F. Izumi, *J. Appl. Crystallogr.* **41**, 653 (2008).
- ³²S. Nandi, A. Kreyssig, L. Tan, J. W. Kim, J. Q. Yan, J. C. Lang, D. Haskel, R. J. McQueeney, and A. I. Goldman, *Phys. Rev. Lett.* **100**, 217201 (2008).
- ³³M. Fiebig, C. Degenhardt, and R. V. Pisarev, *Phys. Rev. Lett.* **88**, 027203 (2001).
- ³⁴T. Lottermoser and M. Fiebig, *Phys. Rev. B* **70**, 220407(R) (2004).